GEOPHYSICS, VOL. 73, NO. 5 (SEPTEMBER-OCTOBER 2008); P. VE13–VE23, 10 FIGS., 1 TABLE.
10.1190/1.2956427

Nonlinear 3D tomographic least-squares inversion of residual moveout in Kirchhoff prestack-depth-migration common-image gathers

Frank Adler[1], Reda Baina[2], Mohamed Amine Soudani[1], Pierre Cardon[1], and Jean-Baptiste Richard[1]

ABSTRACT

Velocity-model estimation with seismic reflection tomography is a nonlinear inverse problem. We present a new method for solving the nonlinear tomographic inverse problem using 3D prestack-depth-migrated reflections as the input data, i.e., our method requires that prestack depth migration (PSDM) be performed before tomography. The method is applicable to any type of seismic data acquisition that permits seismic imaging with Kirchhoff PSDM. A fundamental concept of the method is that we dissociate the possibly incorrect initial migration velocity model from the tomographic velocity model. We take the initial migration velocity model and the residual moveout in the associated PSDM common-image gathers as the reference data. This allows us to consider the migrated depth of the initial PSDM as the invariant observation for the tomographic inverse problem. We can therefore formulate the inverse problem within the general framework of inverse theory as a nonlinear least-squares data fitting between observed and modeled migrated depth. The modeled migrated depth is calculated by ray tracing in the tomographic model, followed by a finite-offset map migration in the initial migration model. The inverse problem is solved iteratively with a Gauss-Newton algorithm. We applied the method to a North Sea data set to build an anisotropic layer velocity model.

INTRODUCTION

We present a new method of 3D reflection tomography with the aim of building velocity-depth models for depth conversion and prestack depth migration (PSDM). The principle of the method is to use PSDM reflections of a possibly incorrect velocity-depth model as the input data for the nonlinear least-squares problem of reflection tomography. The main difference compared with previous methods, which also use PSDM reflections as input for tomography, is that we define depth-migrated reflections from an initial PSDM as invariant observables of a nonlinear least-squares data-fitting problem in the depth domain. We demonstrate that our formulation of the inverse problem is equivalent to nonlinear least-squares fitting of prestack traveltimes in classic reflection tomography (e.g., Bishop et al., 1985) because of the one-to-one relationship between unmigrated and migrated locally coherent events in the framework of Kirchhoff migration (Liu and Bleistein, 1995; Adler, 2002). However, working with depth-domain data has several advantages.

PSDM and migration velocity analysis (MVA)

PSDM is a very powerful seismic imaging technique because it simultaneously solves the focusing and positioning problems of seismic prestack imaging when an accurate velocity-depth model is provided. The construction of a correct velocity model is therefore the most important task of a depth-imaging project. The focusing quality of a velocity-depth model can be measured directly during migration velocity analysis (MVA) of PSDM common-image gathers (CIGs). When the velocity-depth model correctly focuses the seismic data, all primary reflections are aligned horizontally in all CIGs as a function of offset or reflection angle. In the case of a wrong velocity model, we observe a misalignment of reflections that we call residual moveout (RMO).

PSDM is an excellent MVA tool because of its strong sensitivity to the velocity model, which can be quantified for Kirchhoff PSDM (Adler, 2002; Iversen, 2006). Many techniques for velocity-model updating with MVA criteria have been developed (see Stork, 1992 for a comprehensive review of these methods). However, a difficulty of MVA velocity-model updating is that correct focusing alone does not guarantee the correct position of a reflector image in depth. Other criteria must be added, e.g., geologic constraints such as well mark-

Manuscript received by the Editor 29 November 2007; revised manuscript received 15 February 2008; published online 1 October 2008.
[1]TOTAL, Centre Scientifique et Technique Jean Feger, Pau, France. E-mail: frank.adler@total.com; mohamed-amine.soudani@total.com; pierre.cardon@total.com; jeanbaptiste.richard@total.com.
[2]Organisme Pétrolier de Recherche Appliquée, Pau, France. E-mail: reda.baina@univ-pau.fr.

ers or an a priori velocity model. These criteria can be integrated easily in velocity-model updating when the process is formulated as an inverse problem, such as reflection-traveltime tomography.

Tomographic methods

There are at least three major reasons why tomographic methods are suitable for PSDM velocity model building. First, PSDM is required for correct imaging in strongly heterogeneous velocity models in which raypath bending is very strong and spatially varying. Hence, the nonlinearity of traveltimes with respect to velocity is significant, and we have to solve a fully nonlinear inverse problem. The strength of tomography is that it solves the nonlinear inverse problem globally by updating the heterogeneous velocity model until all modeled raypaths explain observed traveltimes. If the model can explain observed traveltimes, we obtain flat events in CIGs (Ehinger and Lailly, 1995). Second, traveltime modeling by ray tracing allows implementing tomography in three dimensions for any configuration in the seismic data acquisition, e.g., marine streamer, land, ocean-bottom cable (OBC), multiazimuth, wide azimuth, and well seismic (e.g., Chiu and Steward, 1987). Third, the nonseismic data can be added to the formulation of the inverse problem (Le Stunff and Grenier, 1998; Sexton, 1998).

Reflection-traveltime tomography (e.g., Bishop et al., 1985; Chiu and Steward, 1987) was developed for velocity-model building long before 3D PSDM was used routinely in the industry. The principle of reflection-traveltime tomography is borrowed from the general concept of data fitting in inverse theory (Tarantola, 1987; Menke, 1989): Find a model $\mathbf{m}$ that matches the modeled data $d(\mathbf{m})$ with the observed data d^{obs} that are invariants of the inverse problem, i.e., they are independent of the unknown model $\mathbf{m}$ to be determined. The mismatch is often measured with the least-squares norm $\|\cdot\|^2$.

Traveltime inversion has two very important practical advantages. First, using the invariant traveltime data t^{obs} allows solving the nonlinear inverse problem iteratively by linear inversions, for example, with the Gauss-Newton scheme. As a consequence, the initial tomographic model can be very different from the optimal solution. Second, the correctness of any model update can be controlled by evaluating the mismatch between $t(\mathbf{m})$ and t^{obs} without repeating PSDM and MVA with the updated model. This direct quality control (QC) is very powerful for testing suitable model architectures (blocky or smooth) and their optimal parameterization (e.g., number of unknowns, regularization weights, a priori weights, etc.) to balance the trade-off between model mismatch errors (the model cannot describe the data) and model estimation errors (resulting, for example, when fitting noise with a very flexible model). This trade-off also is known as underfitting versus overfitting (Gershenfeld, 1999; Li and Oldenburg, 1999; van Wijk et al., 2002).

Despite these advantages, prestack reflection traveltime tomography has never been used routinely in the industry because picking prestack traveltimes on data with low signal-to-noise level or on large 3D data sets is considered almost unfeasible, particularly on complex seismic data for which precise PSDM and tomographic methods are deemed necessary. A second apparent disadvantage of reflection tomography is that it requires continuous reflectors, covering the model partly or completely, for finite-offset ray tracing. A convenient way of defining these reflectors is by seismic interpretation of geologic horizons in the zero-offset time domain (in practice, the stack domain). In the case of time interpretation, we can map them conveniently into the initial tomographic model by normal ray map migration (see, e.g., Robein, 2003 for a review of depth conversion techniques). It turns out that interpreted horizons are valuable and sometimes necessary geologic constraints for the velocity model, as when defining a layered model.

The major challenge for applying reflection traveltime tomography is access to kinematic seismic information, such as prestack traveltimes and interpreted horizons (Apostoiu-Marin and Ehinger, 1997). Many methods have been proposed to improve the efficiency of reflection tomography. We review methods that use unmigrated and migrated seismic data as a starting point.

Tomography with the unmigrated data

A first strategy is to access kinematic data in the unmigrated time domain with automated processing methods, replacing cumbersome interpretive picking of horizons and traveltimes. There are two categories of methods. The first category is based on moveout analysis tools such as stacking velocity analysis (Guiziou et al., 1996; Sexton, 1998) or common-reflection-surface (CRS) stacking (Duveneck, 2004); these provide kinematic wavefront attributes suitable for 3D tomographic inversion. However, these techniques assume short-spread hyperbolic moveout. Tomographic stacking velocity inversion is extended to higher-order moveout by Williamson et al. (1999).

The second category is based on picking locally coherent events by local slant stacking. Locally coherent events were first used for tomography by Sword (1987) and later by Billette and Lambaré (1998) and Chalard (2002) for a technique called stereotomography. These techniques do not make assumptions on moveout, but the automated picking might not be robust enough and requires careful QC. Lavaud et al. (2004) propose making stereotomography more robust by reconstructing locally coherent events from CRS attributes. CRS-based tomography and stereotomogaphy are sometimes limited by the fact that they are designed for smooth velocity models because of the avoidance of continuous horizons. Despite these efforts, time-domain tomographic methods are rarely used for PSDM projects.

Tomography with the migrated data

Another strategy is to access the kinematic data in the migrated domain (in time or depth). Presently, migrated seismic images are always available for interpretation on industry projects. Many authors (e.g., van Trier 1990; Stork, 1992; Whitcombe, 1994; Ehinger and Lailly, 1995; Adler, 1996; Liu, 1997; Sexton, 1998) point out that the migrated domain is most suitable for accessing kinematic data for time-depth mapping and tomography.

It follows from ray theory and Kirchhoff migration theory (e.g., Bleistein, 1987) that unmigrated locally coherent events are connected one-to-one with migrated locally coherent events (time or depth). This is expressed mathematically by equations for finite-offset map migration (van Trier, 1990) or, equivalently, by the kinematic imaging equations (Liu and Bleistein, 1995). As a consequence, unmigrated or migrated events provide equivalent information for tomography.

Because migration simplifies the seismic image, even for quite incorrect velocity models, RMO in migrated CIGs is mostly well behaved and can be picked efficiently in an automated manner (e.g., Woodward et al., 1998; Lemaistre et al., 2001). The reflecting interface required for ray tracing in tomography can be obtained from interpreting the RMO-corrected stack after prestack migration (in time or depth), which is followed by a zero-offset demigration (in time or depth) and a normal ray-map migration (Whitcombe, 1994; Sexton, 1998; Adler et al., 2005). Most importantly, the kinematic data access from migrated 3D CIGs and interpretation on postmigration stacks is feasible in the time frame of industrial projects. We also adopt this strategy for our method.

One issue remains: how to formulate the nonlinear tomographic inverse problem with the migrated seismic data.

Solving the nonlinear inverse problem

In time migration, the concept of matching invariant observables is directly applicable; the invariant is now the migrated time of prestack time-migrated (PSTM) events because they remain unchanged once the time migration finishes. We can consider the migrated time as an observable because we make our observation (picking, interpretation) on the migrated, i.e., processed, data. Seismic processing transforms our physical observables into what we call processed observables. We can use them as the input data for inverse problems as long as the associated forward modeling includes the effect of the corresponding processing step (Raynaud and Robein, 1998). Once we accept this idea, the concept of traveltime inversion is extended easily to the time-migrated data, e.g., after dip moveout (DMO) or PSTM, the ray tracing in the tomographic model is followed by finite-offset map migration, providing modeled prestack migrated times (Raynaud and Robein, 1998; Sexton, 1998; Adler et al., 2005).

The time-migration velocity model is used only as a parameter for map migration in forward modeling; the unknown of the inverse problem is a velocity-depth model. The nonlinear inverse problem matches the migrated time of modeled events with the migrated time of picked (observed) migrated events and can be solved iteratively. Observed migrated times are reconstructed in a horizon-consistent manner from the interpretation (migrated zero-offset) and from automatically picked NMO after DMO or RMO after PSTM (see Robein, 2003 for a review of time imaging methods). These methods work well for high-precision depth-conversion tasks with moderately complex velocity models (Sexton et al., 2000; Adler et al., 2008).

In the case of depth-migrated data, we encounter the difficulty that the position of a migrated event depends, of course, on the velocity-depth model to be determined. Two approaches in the literature handle this problem. The first approach reconstructs invariant prestack traveltimes T^{obs} from PSDM events via ray tracing, which represents a kinematic demigration (Ehinger and Lailly, 1995; Jacobs et al., 1995). This approach enables nonlinear traveltime inversion, but it requires time-consuming interpretation of horizons in the prestack domain before demigration can be performed. The second approach uses an optimization criterion when formulating the inverse problem, based on depth-migration kinematics such as focusing or flatness of events. Within this approach, we can distinguish two methods.

The first method applies a linear inversion after PSDM and RMO analysis (Stork, 1992), minimizing the residual depth error Δz (RMO) for all offsets. Stork (1992) shows that the depth error is converted easily into a traveltime misfit so that a standard algorithm for traveltime inversion can be used. Such an approach is very practical with 3D data because it allows horizon interpretation in the postmigrated stack domain and automated RMO analysis for the data access. This kind of method is probably the most widely used in the industry.

Chauris et al. (2002a, 2002b) propose a flatness criterion of locally coherent events in PSDM CIGs for the linear tomographic inversion. However, they develop their method in only two dimensions, and it suffers from the same limitations as stereotomography (quality control of automated picking, smooth velocity models only). As we demonstrate later, these linear inversion methods do not account for invariant observables. As a consequence, we cannot control the quality of the model update without performing another PSDM and RMO analysis. Another limitation is that linear tomography only provides a correct model when the initial model is already close to the solution. Otherwise, we have to iterate through the so-called PSDM cycle (Figure 1a) to solve the nonlinear inverse problem, which is very expensive.

The second method avoids the PSDM cycle by remigrating the kinematic data after each model update to solve the nonlinear inverse problem iteratively by minimizing the mismatch between kinematically remigrated events (van Trier, 1990; Liu, 1997; Woodward et al., 1998; Guillaume et al., 2004; Wang et al., 2006). All methods of the second approach use the input data (migrated depth errors, migrated positions) that depend on the unknown of the inverse problem (velocity model). Consequently, corresponding objective functions do not contain the invariant data d^{obs}.

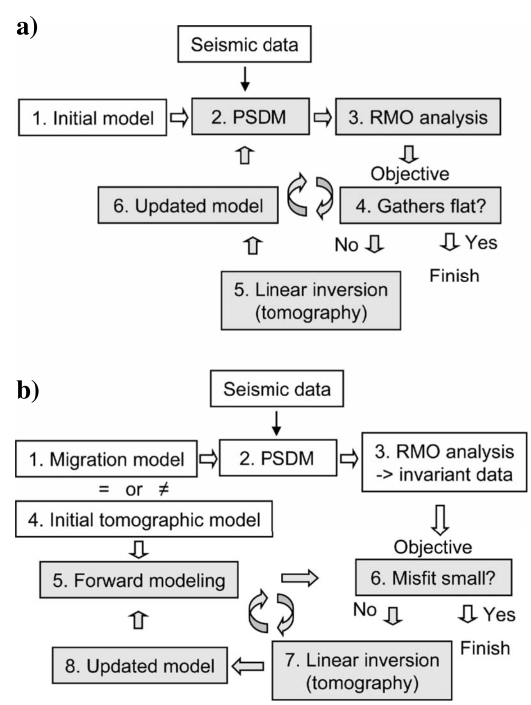

Figure 1. Comparison between (a) PSDM cycle and (b) nonlinear tomography.

In our method of nonlinear reflection tomography with depth-migrated data, we use migrated depth in CIGs as the invariant observable z^{obs} in the inverse problem. The motivation for this development is threefold. First, we prefer to formulate the inverse problem as data fitting to invariants such as traveltime tomography because we gain all of its advantages. Second, the nonlinear time-domain tomography after DMO or PSTM was very successful in determining accurate velocity-depth models for structural uncertainty estimation (Sexton et al., 2000) and drilling applications (Adler et al., 2008). Therefore, we expect similar results with PSDM data. Third, the data-fitting approach enables us to solve another important practical problem that we have not yet mentioned: changing the architecture of a velocity-depth model during a depth-imaging project.

In practice, this problem arises when, for example, a blocky model best represents the geology but a previous PSDM was run with a smooth model, such as Kirchhoff depth migration that requires smoothing of blocky velocity models. The smoothing can lead to inconsistent reflector depths between the blocky velocity model and depth image when velocity contrasts are strong. As a consequence, Kirchhoff PSDM CIGs might exhibit slightly unflattened events, even though reflector depths of the blocky model would be correct when they match well markers. As we demonstrate with our field data example, our method enables us to build correct blocky models using data from a Kirchhoff PSDM, which requires smooth velocity models.

The basic concept of our method is to dissociate the migration model $\mathbf{m}_G$ from tomographic velocity model $\mathbf{m}$, i.e., the method operates with two distinct velocity models. As a consequence, we are free to choose model $\mathbf{m}_G$ as the initial model for $\mathbf{m}$ or a completely different model (Figure 1b). The subscript G in $\mathbf{m}_G$ reminds us that migration kinematics are provided by Green's functions of Kirchhoff depth migration. We use an initial PSDM with a possibly incorrect model $\mathbf{m}_G$ as the reference data set that provides the observed depth $z^{\mathrm{obs}}(\mathbf{m}_G)$ to which we match modeled migrated depth $z(\mathbf{m}_G,\mathbf{m})$. For example, we use a smooth velocity model $\mathbf{m}_G$ for an initial Kirchhoff depth migration and construct a blocky velocity model $\mathbf{m}$ that ties well markers, which is suitable for wave-equation depth migration. The model $\mathbf{m}_G$ is kept unchanged during the velocity-model-building process.

Within the framework of the method of Raynaud and Robein (1998), we use only the migration model to perform a finite-offset map migration exactly reproducing kinematics of the PSDM algorithm applied to the seismic data. Therefore, we can compare the modeled data (migrated depth) in the domain in which we made observations (RMO analysis in PSDM CIGs). With this approach, we can solve the nonlinear inverse problem iteratively by least-squares data-fitting in complete analogy to traveltime inversion (Figure 1b). The input data are RMO values and horizons interpreted on the RMO-corrected stack of the initial PSDM. The forward modeling adds a finite-offset map migration after ray tracing, but this is still much faster than a PSDM and RMO analysis.

In the following sections, we first recall principles of classic reflection traveltime inversion and linear tomography in depth after MVA. Then we explain forward modeling with ray tracing and finite-offset map migration. Finally, we present the formulation of the nonlinear inverse problem and show an application of our method to a North Sea data set in which we built a vertical transversely isotropic (VTI) velocity model starting from an initial PSDM using a simple 1D isotropic model.

NONLINEAR INVERSION OF REFLECTION TRAVELTIMES

Classic reflection tomography (e.g., Bishop et al., 1985) is formulated as an inverse problem of fitting invariant (picked) prestack traveltimes T^{obs} in the least-squares sense. The objective function to be minimized with respect to the model $\mathbf{m}$ is

$$C(\mathbf{m}) = \|T^{\mathrm{obs}} - T(\mathbf{m})\|^2. \tag{1}$$

Here, the tomographic model $\mathbf{m}$ is a combination of velocity and reflector models (e.g., Ehinger and Lailly, 1995). To keep formulas simple, we neglect possible weights or covariance matrices and additional terms in the objective function, such as regularization terms, a priori terms, or other misfit terms (e.g., geologic constraints). Because the traveltime function $T(\mathbf{m})$ is nonlinear in $\mathbf{m}$, the classic method to solve the inverse problem is to linearize the traveltime function and to minimize the objective function,

$$\begin{aligned} C(d\mathbf{m}) &= \left\| T^{\mathrm{obs}} - T(\mathbf{m}) - \frac{\partial T(\mathbf{m})}{\partial^t \mathbf{m}} d\mathbf{m} \right\|^2 \\ &= \left\| \Delta t(\mathbf{m}) - \frac{\partial T(\mathbf{m})}{\partial^t \mathbf{m}} d\mathbf{m} \right\|^2 \end{aligned} \tag{2}$$

with respect to a perturbation $d\mathbf{m}$ of the model $\mathbf{m}$.

Because T^{obs} is invariant or model independent, we can exactly calculate the misfit of the updated model

$$\Delta t(\mathbf{m} + d\mathbf{m}) = T^{\mathrm{obs}} - T(\mathbf{m} + d\mathbf{m}) \tag{3}$$

and solve the nonlinear inverse problem iteratively with equation 2 in a Gauss-Newton algorithm. As shown below, this is not possible with linear tomography after MVA in the depth domain.

LINEAR TOMOGRAPHY IN DEPTH AFTER MVA

Depth-migrated data usually allow interpretation of horizons as single-valued functions even when the velocity model is wrong. Without loss of generality, we assume in the following that we have migrated data in the common-offset domain, denoted by half-offset h. It is very convenient to define reflector interfaces for reflection tomography by the imaged depth $z(h = 0, x, y, \mathbf{m}_G) = z(h_0, \mathbf{m}_G)$ of a reflection in the stack after PSDM. Tomographic methods based on MVA criteria (e.g., Stork, 1992; Chauris et al., 2002a, 2002b) naturally assume the migration and tomographic models are identical, i.e., $\mathbf{m} = \mathbf{m}_G$. Modeled traveltimes $T(h, z(h_0, \mathbf{m}), \mathbf{m})$ (Figure 2b) therefore depend only on the velocity model $\mathbf{m}$. The dependency of the horizon $z(h_0, \mathbf{m})$ on $\mathbf{m}$ can be handled with normal ray remigration respecting the invariant zero-offset traveltime (e.g., Biondi, 2006). No separate interface model is required as in classic reflection tomography. As pointed out by van Trier (1990), this has the advantage of having fewer unknowns, and it avoids handling unknowns with different physical dimensions.

The objective of linear tomography is to minimize depth errors $\Delta z(h, \mathbf{m})$ picked after PSDM, for instance, by an automated RMO analysis of events $z(h,\mathbf{m})$ (Figure 2a). The corresponding unmigrated traveltime data are $T^{\mathrm{obs}} = T(h,z(h,\mathbf{m}),\mathbf{m})$. Because we trace all finite-offset rays for tomography from the zero-offset imaged depth $z(h_0,\mathbf{m})$ (horizon), we cannot reconstruct exactly the observed finite-offset traveltime (Figure 2b), but we can approximate T^{obs} by reconstructing the imaged depth $z(h,\mathbf{m}) = z(h_0,\mathbf{m}) + \Delta z(h,\mathbf{m})$:

$$\begin{aligned} T^{\mathrm{obs}}(h) &= T(h,z(h_0,\mathbf{m}) + \Delta z(h,\mathbf{m}),\mathbf{m}) \\ &\approx T(h,z(h_0,\mathbf{m}),\mathbf{m}) + \frac{\partial T(h,z(h_0,\mathbf{m}),\mathbf{m})}{\partial z}\Delta z(h,\mathbf{m}) \\ &= T(h,z(h_0,\mathbf{m}),\mathbf{m}) + \Delta t(h,\mathbf{m}), \end{aligned} \tag{4}$$

with

$$\Delta t(h,\mathbf{m}) = \frac{\partial T(h,z(h_0,\mathbf{m}),\mathbf{m})}{\partial z}\Delta z(h,\mathbf{m}). \tag{5}$$

Equation 5 is equivalent to equation 1c of Stork (1992). Following equation 2, we can formulate the inverse problem in the time domain with the linearized objective function:

$$C(d\mathbf{m}) = \left\| T^{\mathrm{obs}}(h) - T(h,z(h_0,\mathbf{m}),\mathbf{m}) - \left(\frac{\partial T(h,\mathbf{m})}{\partial^t \mathbf{m}} + \frac{\partial T(h,\mathbf{m})}{\partial z}\frac{\partial z(h_0,\mathbf{m})}{\partial^t \mathbf{m}} \right) d\mathbf{m} \right\|^2. \tag{6}$$

However, our approximated T^{obs} in equation 4 is not an invariant. From equations 4–6 follows

$$C(d\mathbf{m}) = \left\| \Delta t(h,\mathbf{m}) - \left(\frac{\partial T(h,z(h_0,\mathbf{m}),\mathbf{m})}{\partial^t \mathbf{m}} + \frac{\partial T(h,z(h_0,\mathbf{m}),\mathbf{m})}{\partial z}\frac{\partial z(h_0,\mathbf{m})}{\partial^t \mathbf{m}} \right) d\mathbf{m} \right\|^2. \tag{7}$$

The objective function in equation 7 has the same form as equation 2, but we cannot exactly calculate a misfit residual of the updated model as in equation 3. Instead, a new PSDM and RMO analysis must be performed to evaluate the correctness of the updated velocity model. We note, however, that the new imaged depth of the interpreted horizon $z(h_0,\mathbf{m} + d\mathbf{m})$ can be predicted exactly with normal ray remigration, so we do not need to reinterpret the postmigration stack of the updated model. This result also is useful for nonlinear iterative methods (see Figure 5 for examples).

To extend the linear MVA tomography to an iterative method, it is necessary to model the new migrated depth in the updated tomographic model via kinematic finite-offset remigration of depth-migrated events. This can be achieved by applying ray tracing (demigration) in the model $\mathbf{m}$ followed by finite-offset map migration in the model $\mathbf{m} + d\mathbf{m}$.

Several methods of kinematic finite-offset remigration appear in the literature. Van Trier (1990) applies a linearization of the curved velocity ray (Iversen, 1996; Adler, 2002) in his forward problem. Liu (1997) and Woodward et al. (1998) use a linearized vertical perturbation of the imaged depth $z(h,\mathbf{m})$ to formulate the objective function minimization within CIG locations. Guillaume et al. (2004) and Wang et al. (2006) apply a demigration of locally coherent depth-migrated events in the migration model $\mathbf{m}_G$ followed by exact 3D finite-offset map migration in tomographic model $\mathbf{m} + d\mathbf{m}$. To our knowledge, the last method is the first 3D depth-domain tomography method that dissociates the migration velocity model from the tomographic model. The associated inverse problems of these forward-modeling methods all try to minimize distances between remigrated events, i.e., they are based on MVA criteria (event flattening or focusing). The formulation of the inverse problem of our method is fundamentally different from those methods because we use a data-fitting criterion for invariant observed migrated depth z^{obs}.

NONLINEAR INVERSION OF INVARIANT DEPTH-MIGRATED REFLECTIONS

We formulate in the following the forward-modeling and inverse problem of our tomographic inversion method.

Forward modeling with finite-offset map migration

Forward modeling consists of two steps: first, we trace rays on horizons in the tomographic model $\mathbf{m}$; second, we apply exact 3D finite-offset map migration in the migration model $\mathbf{m}_G$ to the modeled data. This approach provides flexibility in our choice of model architectures for tomographic model $\mathbf{m}$ (blocky or smooth). The map migration reproduces kinematics of the PSDM that was applied to the seismic data (Raynaud and Robein, 1998).

Our fundamental equation for finite-offset map migration is the imaging condition (Liu and Bleistein, 1995; Liu, 1997; Adler, 2002) of Kirchhoff depth migration:

$$\begin{aligned} T^{\mathrm{obs}}(\mathbf{x}_S,\mathbf{x}_R) &= T_G(\mathbf{x}_S,\mathbf{x}_R,\mathbf{x}_G^{\mathrm{obs}},\mathbf{m}_G), \\ p_\xi^{\mathrm{obs}}(\mathbf{x}_S,\mathbf{x}_R) &= p_{G,\xi}(\mathbf{x}_S,\mathbf{x}_R,\mathbf{x}_G^{\mathrm{obs}},\mathbf{m}_G), \\ p_\eta^{\mathrm{obs}}(\mathbf{x}_S,\mathbf{x}_R) &= p_{G,\eta}(\mathbf{x}_S,\mathbf{x}_R,\mathbf{x}_G^{\mathrm{obs}},\mathbf{m}_G). \end{aligned} \tag{8}$$

This equation is equivalent to the stationary-phase condition of Kirchhoff migration (Bleistein, 1987) and states that the reflector image point $\mathbf{x}_G^{\mathrm{obs}} = (\mathbf{x}_G^{\mathrm{obs}},\mathbf{y}_G^{\mathrm{obs}},\mathbf{z}_G^{\mathrm{obs}})$, in model $\mathbf{m}_G$ is connected one-to-one with the recorded locally coherent reflection event $(T^{\mathrm{obs}},p_\xi^{\mathrm{obs}},p_\eta^{\mathrm{obs}})$ via a pair of specular rays defined by $(T_G,p_{G,\xi},p_{G,\eta})$ from Green's functions. The recorded and modeled traveltime data share the same source and receiver locations $\mathbf{x}_S$ and $\mathbf{x}_R$. Quantities $p_{G,\xi}$, and $p_{G,\eta}$ are the horizontal slownesses or traveltime derivatives of Green's functions. Coordinates ξ and η represent integration coordinates of Kirchhoff PSDM that depend on the imaging configuration as follows:

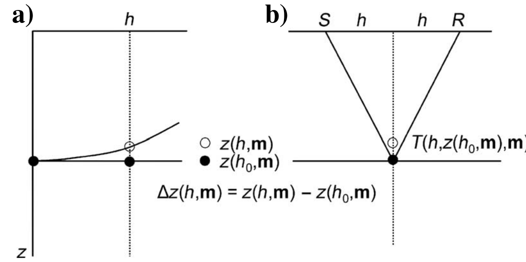

Figure 2. Linear tomography after MVA. (a) CIG with a curved event having RMO $\Delta z(h,\mathbf{m})$. (b) Forward modeling with ray tracing on zero-offset migrated depth (horizon) $z(h_0,\mathbf{m})$.

$$\text{Common shot: } (\xi,\eta) = (x_R, y_R), \quad p_\xi = p_{x_R} = \frac{\partial T}{\partial x_R},$$
$$p_\eta = p_{y_R} = \frac{\partial T}{\partial y_R};$$

$$\text{Common receiver: } (\xi,\eta) = (x_S, y_S), \quad p_\xi = p_{x_S} = \frac{\partial T}{\partial x_S},$$
$$p_\eta = p_{y_S} = \frac{\partial T}{\partial y_S};$$

$$\text{Common offset: } (\xi,\eta) = \left(\frac{x_S + x_R}{2}, \frac{y_S + y_R}{2}\right),$$
$$p_\xi = p_{x_S} + p_{x_R},$$
$$p_\eta = p_{y_S} + p_{y_R}.$$

Equation 8 represents a bijective map between an observed time event and its corresponding image point we observe in depth. In this sense, we attach the superscript *obs* at the image point $\mathbf{x}_G^{obs}$, stressing the fact that the image point will constitute our invariant observable in the inverse problem, although it depends on a possibly incorrect migration velocity model. This is valid because the migration velocity remains invariant while solving the inverse problem. The RMO-corrected stack after the initial PSDM is used for horizon interpretation. Because our initial tomographic model $\mathbf{m}$ can be different from $\mathbf{m}_\mathrm{G}$, we map each horizon into the initial tomographic model with normal rays. We represent a horizon by $z(h_0,\mathbf{m}) = z(h_0,x,y,\mathbf{m})$.

For our forward problem, we apply the imaging condition to the modeled data, i.e., after shooting specular ray pairs in our tomographic model $\mathbf{m}$ from the horizon $z(h_0,\mathbf{m})$ that emerge at surface locations $\mathbf{x}_\mathrm{S}$ and $\mathbf{x}_\mathrm{R}$:

$$\begin{aligned} T(\mathbf{x}_S,\mathbf{x}_R,z(h_0,\mathbf{m}),\mathbf{m}) &= T_G(\mathbf{x}_S,\mathbf{x}_R,\mathbf{x}_G,\mathbf{m}_G),\\ p_\xi(\mathbf{x}_S,\mathbf{x}_R,z(h_0,\mathbf{m}),\mathbf{m}) &= p_{G,\xi}(\mathbf{x}_S,\mathbf{x}_R,\mathbf{x}_G,\mathbf{m}_G),\\ p_\eta(\mathbf{x}_S,\mathbf{x}_R,z(h_0,\mathbf{m}),\mathbf{m}) &= p_{G,\eta}(\mathbf{x}_S,\mathbf{x}_R,\mathbf{x}_G,\mathbf{m}_G). \end{aligned} \tag{9}$$

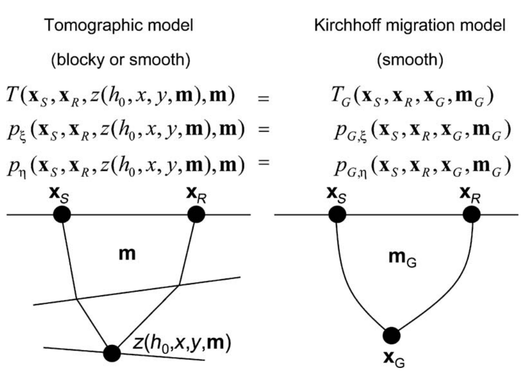

Figure 3. Correspondence between (a) reflection event in tomographic model and (b) image point $\mathbf{x}_\mathrm{G}$ in migration model when traveltimes and their derivatives are identical for both raypaths.

As a consequence, an image point $\mathbf{x}_\mathrm{G}$ in the migration model $\mathbf{m}_\mathrm{G}$ depends on model $\mathbf{m}$ because it is connected via the imaging condition to a reflection point in the tomographic model $\mathbf{m}$ (Figure 3). It follows from equations 8 and 9 that our tomographic model $\mathbf{m}$ matches recorded reflection events $(T^{\mathrm{obs}}, p_\xi^{\mathrm{obs}}, p_\eta^{\mathrm{obs}})$ when the imaging condition for the ray-traced data (equation 9) yields the image point $\mathbf{x}_G^{\mathrm{obs}}$. It is important to note that we do not formulate the inverse problem as matching a modeled point $\mathbf{x}_\mathrm{G}$ to a specific point $\mathbf{x}_G^{\mathrm{obs}}$ as, for example, in stereotomography (Billette and Lambaré, 1998), which tries to match a modeled locally coherent event $(T^{\mathrm{mod}}, p_\xi^{\mathrm{mod}}, p_\eta^{\mathrm{mod}})$ to a particular observed one $(T^{\mathrm{obs}}, p_\xi^{\mathrm{obs}}, p_\eta^{\mathrm{obs}})$. Because we use the horizon-consistent data, we assume we always find a point $\mathbf{x}_G^{\mathrm{obs}}$ at the modeled point $\mathbf{x}_\mathrm{G}$ (through interpolation if necessary) so that we have immediately $x_\mathrm{G} = x_G^{\mathrm{obs}}$, $y_\mathrm{G} = y_G^{\mathrm{obs}}$ for all modeled points $\mathbf{x}_\mathrm{G}$ (otherwise, a point $\mathbf{x}_\mathrm{G}$ cannot be used for the inverse problem). This leaves us with the task of matching the modeled imaged depth $z_\mathrm{G}(h,x_\mathrm{G},y_\mathrm{G},\mathbf{m})$ with the observed imaged depth $z_\mathrm{G}^{\mathrm{obs}}(h,x_\mathrm{G},y_\mathrm{G},\mathbf{m}_\mathrm{G})$. For simplicity, we neglect the coordinates $x_\mathrm{G}, y_\mathrm{G}$ in $z_\mathrm{G}(h,\mathbf{m})$ and $z_\mathrm{G}^{\mathrm{obs}}(h,\mathbf{m}_\mathrm{G})$.

To solve the forward problem, we calculate the image point $\mathbf{x}_\mathrm{G}$ from equation 9, which represents a nonlinear inverse problem for heterogeneous velocity models. Similar to van Trier (1990), we iteratively search image points for all modeled events by minimizing the following nonlinear objective function in $\mathbf{x}_\mathrm{G}$

$$C(\mathbf{x}_G) = \left\| \begin{pmatrix} T(\mathbf{x}_S,\mathbf{x}_R,z(h_0,\mathbf{m}),\mathbf{m}) - T_G(\mathbf{x}_S,\mathbf{x}_R,\mathbf{x}_G,\mathbf{m}_G) \\ \varepsilon(\mathbf{p}(\mathbf{x}_S,\mathbf{x}_R,z(h_0,\mathbf{m}),\mathbf{m}) - \mathbf{p}_G(\mathbf{x}_S,\mathbf{x}_R,\mathbf{x}_G,\mathbf{m}_G)) \end{pmatrix} \right\|_{L2}, \tag{10}$$

with $\mathbf{p} = (p_\xi, p_\eta)$ and $\mathbf{p}_\mathrm{G} = (p_{\mathrm{G},\xi}, p_{\mathrm{G},\eta})$.

We store quantities $T_\mathrm{G}(\mathbf{m}_\mathrm{G})$ and $\mathbf{p}_\mathrm{G}(\mathbf{m}_\mathrm{G})$ in Green's functions files of the initial PSDM and subsequently use them for the forward problem of tomography. The finite-offset map migration can be implemented efficiently with high-performance computing technology available in the industry.

In summary, we shoot specular finite-offset rays from horizons that provide all quantities of the left-hand side of equation 9 required for finding corresponding image points $\mathbf{x}_\mathrm{G}$. To set up the inverse problem, we collect the observed migrated depth $z_\mathrm{G}^{\mathrm{obs}}(h,\mathbf{m}_\mathrm{G})$ at the modeled CIG location $(x_\mathrm{G}, y_\mathrm{G})$ from the horizon-consistent RMO data.

The inverse problem

The objective of our tomographic inversion method is to match the modeled imaged depth $z_G(h,\mathbf{m})$ with an invariant observed imaged depth $z_G^{\mathrm{obs}}(h,\mathbf{m}_\mathrm{G})$ in the initial migration model that is possibly incorrect.

First, we reconstruct the observed imaged depth from the depth horizon (zero-offset imaged depth) $z_G^{\mathrm{obs}}(h_0,\mathbf{m}_\mathrm{G})$ and the RMO $\Delta z_G^{\mathrm{obs}}(h,\mathbf{m}_\mathrm{G})$ at the modeled CIG location (x_G, y_G):

$$z_\mathrm{G}^{\mathrm{obs}}(h,\mathbf{m}_\mathrm{G}) = z_\mathrm{G}^{\mathrm{obs}}(h_0,\mathbf{m}_\mathrm{G}) + \Delta z_\mathrm{G}^{\mathrm{obs}}(h,\mathbf{m}_\mathrm{G}). \tag{11}$$

Defining the tomographic misfit in a CIG as a function of half-offset h (Figure 4) as

$$\Delta z_{\mathrm{G}}(h,\mathbf{m}) = z_{\mathrm{G}}^{\mathrm{obs}}(h,\mathbf{m}_{\mathrm{G}}) - z_{\mathrm{G}}(h,\mathbf{m}), \tag{12}$$

we formulate the inverse problem as a minimization of the objective function:

$$C(\mathbf{m}) = \| z_{\mathrm{G}}^{\mathrm{obs}}(h,\mathbf{m}_{\mathrm{G}}) - z_{\mathrm{G}}(h,\mathbf{m})\|^2. \tag{13}$$

We can, of course, add more terms to equation 13 (e.g., a term for an a priori model, a regularization term, a geologic constraint, etc.).

To construct the Jacobian of the associated linearized inverse problem, we need Fréchet derivatives of the forward model $z_{\mathrm{G}}(h,\mathbf{m})$ with respect to model parameters $\mathbf{m}$, which we define in Appendix A:

$$\frac{\partial z_{\mathrm{G}}(h,\mathbf{m})}{\partial^t \mathbf{m}} = \left(\frac{\partial T_{\mathrm{G}}(h, z_{\mathrm{G}}(h,\mathbf{m}),\mathbf{m}_{\mathrm{G}})}{\partial z}\right)^{-1}\left(\frac{\partial T(h,\mathbf{m})}{\partial^t \mathbf{m}} + \frac{\partial T(h,\mathbf{m})}{\partial z}\frac{\partial z(h_0,\mathbf{m})}{\partial^t \mathbf{m}}\right). \tag{14}$$

The objective function of the linearized inverse problem is then

$$C(d\mathbf{m}) = \left\| \Delta z_{\mathrm{G}}(h,\mathbf{m}) - \frac{\partial z_{\mathrm{G}}(h,\mathbf{m})}{\partial^t \mathbf{m}} d\mathbf{m}\right\|^2. \tag{15}$$

The method allows an iterative solution of the nonlinear inverse problem because we can calculate the following residual exactly after each model update:

$$\Delta z_{\mathrm{G}}(h,\mathbf{m}+d\mathbf{m}) = z_{\mathrm{G}}^{\mathrm{obs}}(h,\mathbf{m}_{\mathrm{G}}) - z_{\mathrm{G}}(h,\mathbf{m}+d\mathbf{m}). \tag{16}$$

In Appendix B, we show that it is possible to formulate the linearized inverse problem in equation 15 with time residuals, similar to MVA tomography, so that we can use a standard linear solver for traveltime inversion in our method.

APPLICATION TO THE NORTH SEA DATA

We applied our method during a 3D depth-imaging project of an area of about 480 km^2 in the North Sea. Sonic logs and well markers of four wells also were available. Two seismic lines of this area are shown in Figure 5. H1, H2, and H3 define base horizons of corresponding layers. Therefore, both horizons and layers are labeled H1, H2, or H3. We report here the velocity-model construction down to horizon H3 (base of Cretaceous) in Figure 5, which is characterized by fast velocities compared with the overburden. The project was started with an initial PSDM using an isotropic $V0 + kz$ model. Values for $V0$ and k were optimized by MVA to flatten CIGs along horizon H1 only. This 1D model provides good focusing above horizon H1 but is too fast for layer H2 and sometimes too slow below horizon H3 (Figures 8c and 8d, 9c and 9d). Moreover, horizons H2 and H3 are too deep compared with the well markers (Figure 5c), indicating the vertical velocity is too fast.

The well match cannot be improved with a 3D isotropic model, which indicates we need an anisotropic velocity model to explain the seismic and well data. A blocky model using factorized VTI anisotropy (Sexton, 1998; Sarkar and Tsvankin, 2004) for phase velocity $V(\theta,x,y,z) = (V(x,y) + kz)A(\theta,\delta,\varepsilon)$ with phase angle θ and Thomsen's (1986) anisotropic parameters δ and ε was chosen. The $V(x,y)$ maps are represented by B-splines, whereas k, δ, and ε are constant per layer. The blocky model is most suitable for representing strong velocity contrasts at horizons H2 and H3 and for optimizing the well tie between layer boundaries and well markers in the inverse problem (Sexton, 1998).

Let us first assume that we apply the PSDM cycle after the initial PSDM with the $V0 + kz$ model. At least one anisotropic inversion would be required to optimize layer H1. For layer H2, we would need one isotropic PSDM followed by at least one anisotropic PSDM. Layer H3 (Cretaceous) is considered isotropic but with a strong vertical velocity gradient. Updating the Cretaceous layer would require at least one isotropic PSDM. Therefore, we have to run at least four PSDMs for model updating plus a final PSDM to QC

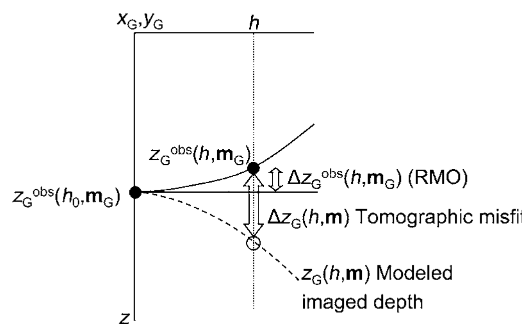

Figure 4. Definition of tomographic misfit in depth-migrated domain.

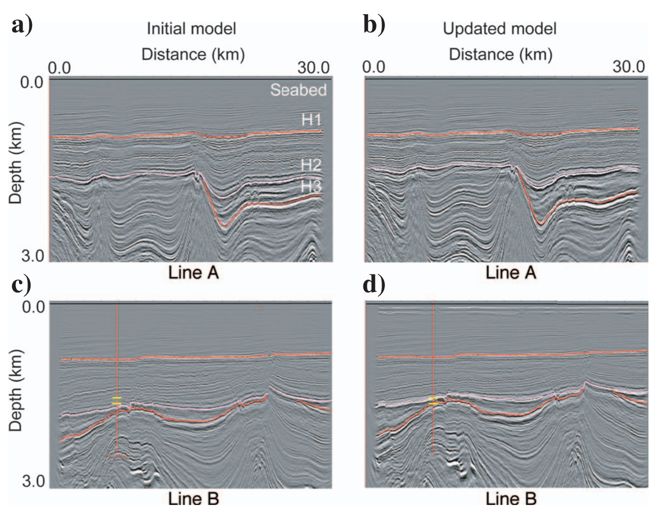

Figure 5. (a) Line A: PSDM postmigration stack from initial model and interpretations that define reflector horizons for tomography. (b) Line A: PSDM postmigration stack from updated model and remigrated horizons. (c) Line B: initial model does not match markers of horizons H2 and H3. (d) Line B: updated anisotropic model better focuses the seismic data and matches the well markers of H2 and H3.

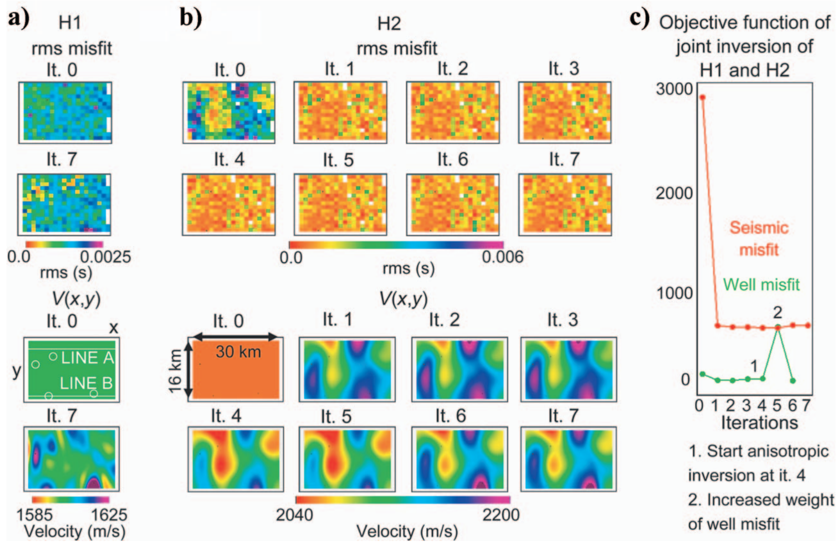

Figure 6. (a) Initial and final rms misfit maps and $V(x,y)$ maps of horizon H1. Circles indicate well locations. (b) Evolution of rms misfit maps and $V(x,y)$ maps for horizon H2 during iterations. (c) Objective function of the joint inversion of layers H1 and H2 (see also Table 1).

Table 1. Evolution of δ, ε, and well tie (average, standard deviation) for layer H2.

			Well tie	
	δ	ε	Average	Standard deviation
Iteration 0	0.07	0.07	39.1 m	41.9 m
Iteration 1	0.07	0.07	10.6 m	12.52 m
Iteration 2	0.07	0.07	8.92 m	10.99 m
Iteration 3	0.07	0.07	8.96 m	11.06 m
Iteration 4	0.08	0.143	11.2 m	12.03 m
Iteration 5	0.797	0.146	10.8 m	11.8 m
Iteration 6	0.067	0.131	0.654 m	0.763 m
Iteration 7	0.068	0.128	0.668 m	0.8 m

the Cretaceous layer. We also assume optimal model parameters are found immediately with each linear tomography. However, this is rarely the case, and several test PSDMs need to be run to optimize the parameterization of tomography (number of unknowns, regularization weights).

With the nonlinear tomography, we can perform the inversion globally or by layer stripping using a blocky model as the initial tomographic model (the initial migration model was smooth). We chose to update layers H1 and H2 jointly (Figure 6 and Table 1). Initial model parameters for $V(x,y)$ and k are average values derived from well logs. For layer H1, we obtained values $V = 2050$ m/s, $k = 0.636$ s^{-1}. For layer H2, we obtained $V = 1600$ m/s, $k = 0.0$ s^{-1}. Initial anisotropy parameters were obtained from regional knowledge and subsequently used as a priori values: $\delta = 0.04$, $\varepsilon = 0.04$ for layer H1 and $\delta = 0.07$, $\varepsilon = 0.07$ for layer H2. During the inversion with seven iterations, for layer H1 we optimized only the $V(x,y)$ map (Figure 6a).

Figure 6b and Table 1 show the evolution of model parameters of layer H2. Each cell of rms misfit maps in Figure 6 displays the rms misfit calculated for all finite-offset ray pairs of a common reflection point on the horizon. Until iteration 3, we tried to optimize only $V(x,y)$ maps, keeping δ and ε as our a priori values, and we obtained a decrease of the seismic misfit term (equation 13) and of a second well misfit term in the global objective function (Figure 6c, Table 1). From iteration 4 onward, we tried to find an anelliptic model for layer H2. We noticed the seismic misfit decreased, but this was not the case for the well misfit (point 1 in Figure 6c). In this situation, we balanced the trade-off between model-mismatch and model-estimation errors with objective-function weights. We chose increasing weights of the well misfit term in the global objective function (point 2 in Figure 6c). At iteration 7, we finally obtained a better well tie, but we slightly increased the seismic misfit. We see here the value of the cost function for analyzing the trade-off between model-mismatch and model-estimation errors.

Finally, we updated $V(x,y)$ and k for layer H3 during 15 iterations (Figure 7). Until iteration 3, we estimated jointly an average constant velocity of $V = 1702$ m/s and a vertical gradient of $k = 1.1218$ s^{-1}. We used these as a priori values for the remaining iterations. At iteration 4 (point 2 in Figure 7c), we also started to invert well misfits and increased their weights at iteration 6, which increased the seismic misfit (point 3 in Figure 7c). Then we reduced the well-misfit weight slightly and refined the $V(x,y)$ B-spline grid progressively until iteration 15.

Below horizon H3, we flooded the model with average values for V and k that were obtained from sonic logs. In Figures 8 and 9, we display lines A and B with the initial and final model. Figure 8 shows a section in which layer H3 is quite thick and is pinching out at layer H2. Figure 9 shows a section in which a well penetrates layer H3. The match between the velocity model and well data is shown in Figure 10. The nonlinear tomography provides an overall improved velocity model with good balance between seismic focusing and well tie. The time savings with respect to the PSDM cycle was estimated to be at least a factor of four.

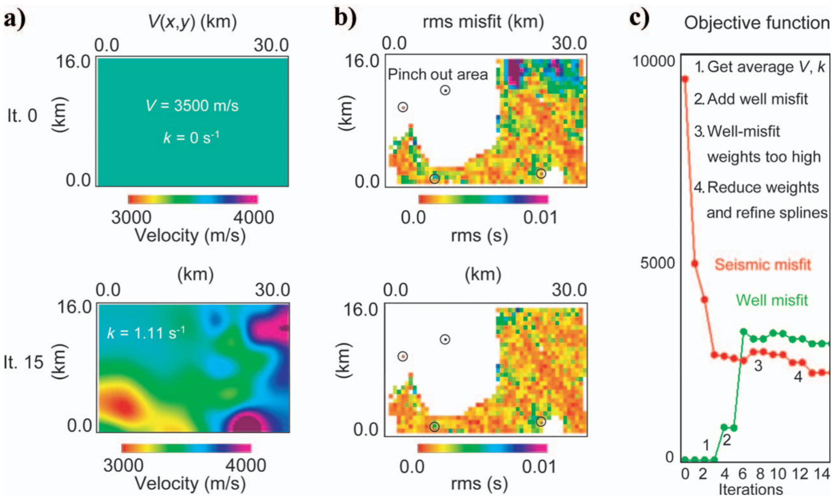

Figure 7. Update of layer H3. (a) $V(x,y)$ maps of initial model (iteration 0) and final model (iteration 15). (b) The rms misfit maps of initial and final model. Circles indicate well locations. (c) Objective function.

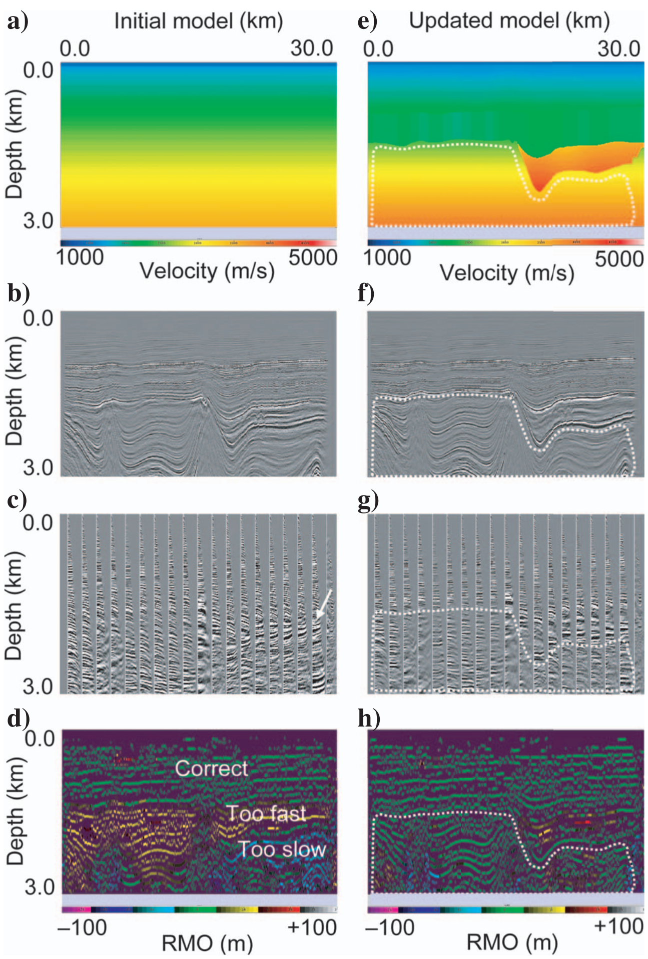

Figure 8. Line A. (a) Initial migration model. (b) Postmigration stack. (c) CIGs of initial model. Note the strong up-and-down curving RMO (arrow). (d) RMO at reference offset 3500 m. (e) Model after nonlinear tomography. The area in the dotted line was not updated with tomography. (f) Postmigration stack with updated model. (g) CIGs with updated model. (h) RMO at reference offset 3500 m.

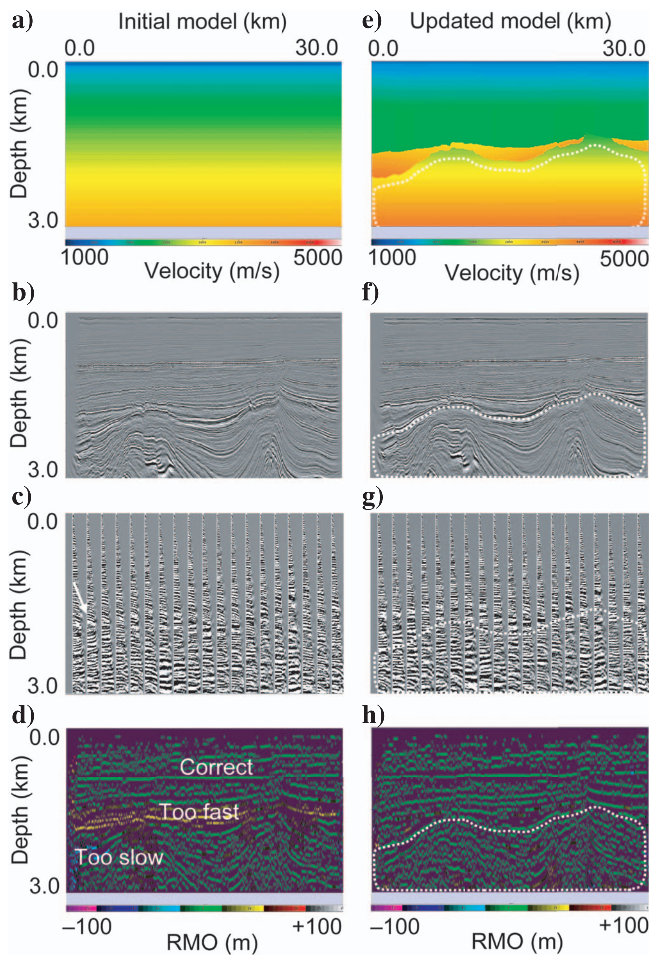

Figure 9. Line B. Example at well location. (a) Initial migration model. (b) Postmigration stack. (c) CIGs of initial model. Note the strong up-and-down curving RMO (arrow). (d) RMO at reference offset 3500 m. (e) Model after nonlinear tomography. The area in the dotted line was not updated with tomography. (f) Postmigration stack with updated model. (g) CIGs with updated model. (h) RMO at reference offset 3500 m.

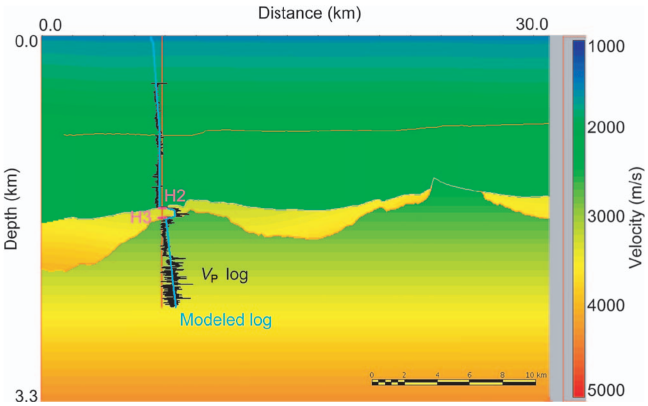

Figure 10. Comparison between velocity model, well markers, and V_P sonic log.

CONCLUSIONS

We have presented a new nonlinear tomographic inversion method using RMO in depth-migrated CIGs of Kirchhoff PSDM. The novelty is that we consider the imaged depth of an initial PSDM as the invariant observable z^{obs} for the nonlinear data fitting in the least-squares sense similar to observed traveltimes T^{obs} in traveltime inversion. Keeping the migrated data as invariants requires dissociating the migration velocity model from the tomographic model. The forward modeling is extended by a finite-offset map migration in the initial, possibly incorrect, migration model, and the tomographic misfit is measured in depth. The linearized inverse problem can be reformulated with time residuals so the method is implemented easily in existing traveltime-inversion algorithms.

We have applied the method successfully to a North Sea data set in constructing an anisotropic VTI velocity-depth model much faster than with the PSDM cycle. On our example, we estimate a gain of a factor of four. Furthermore, the method provides important QC functions, which can be used to optimize model parameterizations and handle the trade-off between model mismatch errors and model estimation errors. Therefore, the method will be suitable for tomographic sensitivity analysis to assess structural uncertainties in PSDM images and to quickly build velocity-depth models for very large seismic data sets, such as wide-azimuth data, in which Kirchhoff depth migration will become very expensive computationally.

ACKNOWLEDGMENTS

We thank Total SA, Total E&P Nederland B.V., and partner Energie Beheer Nederland B.V. for granting permission to publish this article. We also acknowledge the constructive suggestions of François Audebert, Tamas Nemeth, Erik Duveneck, Einar Iversen, and two anonymous reviewers for improving the manuscript.

APPENDIX A

FRÉCHET DERIVATIVES

In this appendix, we discuss the calculation of Fréchet derivatives in equation 14. Because our method is horizon based, we consider only perturbations of traveltime and horizon functions. The starting point is the first equation in equation 9, in which we introduce half-offset h, midpoint (ξ, η), and the model dependency of the modeled imaged depth $z_G(h,\mathbf{m})$:

$$T(h,\xi,\eta,z(h_0,\mathbf{m}),\mathbf{m}) = T_G(h,\xi,\eta,z_G(h,\mathbf{m}),\mathbf{m}_G). \tag{A-1}$$

Introducing a model perturbation $d\mathbf{m}$ in equation A-1,

$$T(h,\xi,\eta,z(h_0,\mathbf{m}+d\mathbf{m}),\mathbf{m}+d\mathbf{m}) = T_G(h,\xi,\eta,z_G(h,\mathbf{m} + d\mathbf{m}),\mathbf{m}_G), \tag{A-2}$$

followed by linearization yields

$$\frac{\partial T(h,\mathbf{m})}{\partial^t \mathbf{m}} + \frac{\partial T(h,\mathbf{m})}{\partial z}\frac{\partial z(h_0,\mathbf{m})}{\partial^t \mathbf{m}} = \frac{\partial T_G(h,z_G(h,\mathbf{m}),\mathbf{m}_G)}{\partial z}\frac{\partial z_G(h,\mathbf{m})}{\partial^t \mathbf{m}} \tag{A-3}$$

and the required Fréchet derivative

$$\frac{\partial z_G(h,\mathbf{m})}{\partial^t \mathbf{m}} = \left(\frac{\partial T_G(h,z_G(h,\mathbf{m}),\mathbf{m}_G)}{\partial z}\right)^{-1}\left(\frac{\partial T(h,\mathbf{m})}{\partial^t \mathbf{m}} + \frac{\partial T(h,\mathbf{m})}{\partial z}\frac{\partial z(h_0,\mathbf{m})}{\partial^t \mathbf{m}}\right). \tag{A-4}$$

APPENDIX B

FORMULATION OF THE LINEARIZED INVERSE PROBLEM IN THE TIME DOMAIN

As shown by Stork (1992) linear MVA tomography can be formulated in the time domain by converting depth errors into time residuals. It is straightforward to apply this concept to the linearized inverse problem in equation 15.

According to Figure 4, the forward-modeled data of tomographic model $\mathbf{m}$ are connected to the point $\mathbf{x}_G$ with depth $z_G(h,\mathbf{m})$. At location (x_G,y_G), we observe the imaged depth $z_G^{obs}(h,\mathbf{m}_G)$ and misfit in depth $\Delta z_G(h,\mathbf{m}) = z_G^{obs}(h,\mathbf{m}_G) - z_G(h,\mathbf{m})$. We reconstruct the corresponding observed traveltime T^{obs} approximately, taking the first equation in equation 8 as a starting point:

$$\begin{aligned} T^{obs}(h,\xi,\eta) &= T_G(h,\xi,\eta,z_G^{obs}(h,\mathbf{m}_G),\mathbf{m}_G) \\ &= T_G(h,\xi,\eta,z_G(h,\mathbf{m}) + \Delta z_G(h,\mathbf{m}),\mathbf{m}_G) \\ &\approx T_G(h,z_G(h,\mathbf{m}),\mathbf{m}_G) + \frac{\partial T_G(h,z_G(h,\mathbf{m}),\mathbf{m}_G)}{\partial z}\Delta z_G(h,\mathbf{m}) \\ &= T_G(h,z_G(h,\mathbf{m}),\mathbf{m}_G) + \Delta t_G(h,\mathbf{m}), \end{aligned} \tag{B-1}$$

with

$$\begin{aligned} \Delta t_G(h,\mathbf{m}) &= \frac{\partial T_G(h,z_G(h,\mathbf{m}),\mathbf{m}_G)}{\partial z}\Delta z_G(h,\mathbf{m}) \\ &= \frac{\partial T_G(h,z_G(h,\mathbf{m}),\mathbf{m}_G)}{\partial z}(z_G^{obs}(h,\mathbf{m}_G) - z_G(h,\mathbf{m})). \end{aligned} \tag{B-2}$$

Applying the linearization principle of traveltime tomography as in equations 2 and 6, we can use the objective function of the linearized inverse problem:

$$C(d\mathbf{m}) = \left\| T^{\text{obs}}(h) - T(h,z(h_0,\mathbf{m}),\mathbf{m}) - \left(\frac{\partial T(h,\mathbf{m})}{\partial^t \mathbf{m}} + \frac{\partial T(h,\mathbf{m})}{\partial z} \frac{\partial z(h_0,\mathbf{m})}{\partial^t \mathbf{m}} \right) d\mathbf{m} \right\|^2. \tag{B-3}$$

Because $T(h,\mathbf{x}_{\mathrm{G}},\mathbf{m}_{\mathrm{G}}) = T(h,z(h_0,\mathbf{m}),\mathbf{m})$ by definition (equation 9), we obtain with equation B-1

$$C(d\mathbf{m}) = \left\| \Delta t_{\mathrm{G}}(h,\mathbf{m}) - \left(\frac{\partial T(h,\mathbf{m})}{\partial^t \mathbf{m}} + \frac{\partial T(h,\mathbf{m})}{\partial z} \frac{\partial z(h_0,\mathbf{m})}{\partial^t \mathbf{m}} \right) d\mathbf{m} \right\|^2. \tag{B-4}$$

Note that $\Delta t_{\mathrm{G}}(h,\mathbf{m})$ in equation B-4 can be recalculated after each iteration because it contains $z_G^{\text{obs}}(h,\mathbf{m}_{\mathrm{G}})$. Comparing equations B-4 and 15 shows that they differ by the factor $(\partial T_G/\partial z)$. Another interesting property of equation B-4 is that the first iteration of our nonlinear inverse problem (equation 13) is equivalent to linear MVA tomography (equation 7) when we choose $\mathbf{m}_{\mathrm{G}}$ as the initial model for $\mathbf{m}$. In this case, the tomographic misfit $\Delta z_{\mathrm{G}}(h,\mathbf{m})$ is equal to the picked RMO $\Delta z_{\mathrm{G}}^{\text{obs}}(h,\mathbf{m}_{\mathrm{G}})$ because the modeled imaged depth $z_{\mathrm{G}}(h,\mathbf{m} = \mathbf{m}_{\mathrm{G}}) = z_{\mathrm{G}}(h_0,\mathbf{m}_{\mathrm{G}})$ is constant (horizontal line in Figure 4).

REFERENCES

Adler, F., 1996, Tomographie de réflexion à partir des images migrées avant addition: Ph.D. dissertation, Université de Pau et des Pays de l'Adour., (in English).

———, 2002, Kirchhoff image propagation: Geophysics, **67**, 126–134.

Adler, F., P. Cardon, and P. Sexton, 2005, Tomographic residual moveout inversion of PreSTM common-image gathers: 67th Annual Conference and Exhibition, EAGE, Extended Abstracts, B039.

Adler, F., A. Cherrett, J. M. Guéméné, S. Gançarski, P. Lays, and H. Bideaud, 2008, Anisotropic velocity model building and depth-imaging for geosteering of extended reach drilling wells: The Leading Edge, **27**, 478–483.

Apostoiu-Marin, I., and A. Ehinger, 1997, Kinematic interpretation in the prestack depth-migrated domain: Geophysics, **62**, 1226–1237.

Billette, F., and G. Lambaré, 1998, Velocity macro-model estimation from seismic reflection data by stereotomography: Geophysical Journal International, **135**, 671–680.

Biondi, B., 2006, 3D seismic imaging: Investigations in geophysics 14: SEG.

Bishop, T. N., K. P. Bube, R. T. Cutler, R. T. Langan, P. L. Love, L. R. Resnick, R. T. Shuey, D. A. Spindler, and H. W. Wyld, 1985, Tomographic determination of velocity and depth in laterally varying media: Geophysics, **50**, 903–923.

Bleistein, N., 1987, On the imaging of reflectors in the earth: Geophysics, **52**, 931–942.

Chalard, E., 2002, Estimation de marco-modèles de vitesse en sismique réflexion par stéréotomographie 3D: Ph.D. dissertation, École des Mines de Paris.

Chauris, H., M. S. Noble, G. Lambaré, and P. Podvin, 2002a, Migration velocity analysis from locally coherent events in 2D laterally heterogeneous media — Part I: Theoretical aspects: Geophysics, **67**, 1202–1212.

———, 2002b, Migration velocity analysis from locally coherent events in 2D laterally heterogeneous media — Part II: Applications on synthetic and real data: Geophysics, **67**, 1213–1224.

Chiu, S. K. L., and R. R. Steward, 1987, Tomographic determination of three-dimensional seismic velocity structure using well-logs, vertical seismic profiles and surface seismic data: Geophysics, **52**, 1085–1098.

Duveneck, E., 2004, 3D tomographic velocity model estimation with kinematic wavefield attributes: Geophysical Prospecting, **52**, 535–545.

Ehinger, A., and P. Lailly, 1995, Velocity model determination by the SMART method — Part 1: Theory: 65th Annual International Meeting, SEG, Expanded Abstracts, 739–742.

Gershenfeld, N., 1999, The nature of mathematical modeling: Cambridge University Press.

Guillaume, P., F. Audebert, N. Chazanoel, V. Dirks, and X. Zhang, 2004, Flexible 3D finite offset tomography model building: 66th Annual Conference and Exhibition, EAGE, Extended Abstacts, D045.

Guiziou, J. L., J. L. Mallet, and R. Madariaga, 1996, 3D seismic reflection tomography on top of the GOCAD depth modeler: Geophysics, **61**, 1499–1510.

Iversen, E., 1996, Derivatives of reflection point coordinates with respect to model parameters: Pure and Applied Geophysics, **148**, 287–317.

——— 2006, Velocity rays for heterogeneous anisotropic media: Theory and implementation: Geophysics, **71**, no.5, T117-T127.

Jacobs, J., D. Sinoquet, and B. Duquet, 1995, Velocity model determination by the SMART method — Part 2: Application: 65th Annual International Meeting, SEG, Expanded Abstracts, 739–742.

Lavaud, B., R. Baina, and E. Landa, 2004, Poststack stereotomography: A robust strategy for velocity model estimation: 66th Annual Conference and Exhibition, EAGE, Extended Abstacts, C022.

Lemaistre, L., C. Hanitzsch, and A. Lehec, 2001, Automatic and continuous image gather analysis after prestack depth migration: 63rd Annual Conference and Exhibition, EAGE, Extended Abstracts.

Le Stunff, Y., and D. Grenier, 1998, Taking into account a priori information in 3D tomography: 68th Annual International Meeting, SEG, Expanded Abstracts, 1875–1878.

Li, Y., and D. W. Oldenburg, 1999, 3D Inversion of DC resistivity data using an L-curve criterion: 69th Annual International Meeting, SEG, Expanded Abstracts, 251–254.

Liu, Z., 1997, An analytical approach to migration velocity analysis: Geophysics, **62**, 1238–1249.

Liu, Z., and N. Bleistein, 1995, Migration velocity analysis: Theory and an iterative algorithm: Geophysics, **60**, 142–153.

Menke, W., 1989, Geophysical data analysis: Discrete inverse theory: Academic Press, Inc.

Raynaud, B., and E. Robein, 1998, Method for modeling kinematic seismic data processed with at least one motion operator: U.S. Patent 5 764 514.

Robein, E., 2003, Velocities, time-imaging and depth imaging in reflection seismic: Principles and methods: EAGE Publications.

Sarkar, D., and I. Tsvankin, 2004, Migration velocity analysis in factorized VTI media: Geophysics, **69**, 708–718.

Sexton, 1998, 3D Velocity-depth model building using surface seismic and well data: Ph.D. dissertation, University of Durham.

Sexton, P., G. Rabary, P. Berthet, and J. M. Guéméné, 2000, Velocity anisotropy: Key to reducing reserves uncertainty in Elgin-Franklin deep high-pressure/high-temperature fields: Offshore Technology Conference, Expanded Abstracts, 12121.

Stork, C., 1992, Reflection tomography in the postmigrated domain: Geophysics, **57**, 680–692.

Sword, C., 1987, Tomographic determination of interval velocities from reflection seismic data: The method of controlled directional reception: Ph.D. dissertation, Stanford University.

Tarantola, A., 1987, Inverse problem theory: Methods for data fitting and model parameter estimation: Elsevier Science Publication Co., Inc.

Thomsen, L., 1986, Weak elastic anisotropy: Geophysics, **51**, 1954–1966.

van Trier, J., 1990, Tomographic determination of structural velocities from depth-migrated seismic data: Ph.D. dissertation, Stanford University.

van Wijk, K., J. A. Scales, W. Navidi, and L. Tenorio, 2002, Data and model uncertainty estimation for linear inversion: Colorado School of Mines, CWP-425 Project Review, CWP-362P.

Wang, B., V. Dirks, P. Guillaume, F. Audebert, and D. Epili, 2006, A 3D subsalt tomography based on wave-equation migration-perturbation scans: Geophysics, **71**, no. 2, E1-E6.

Whitcombe, D., 1994, Fast model building using demigration and single-step ray migration: Geophysics, **59**, 439–449.

Williamson, P. R., P. Sexton, J. Mispel, and P. Berthet, 1999, Anisotropic prestack velocity inversion: A North Africa case study: 69th Annual International Meeting, SEG, Expanded Abstracts, 1592–1595.

Woodward, M., P. Farmer, D. Nichols, and S. Charles, 1998, Automated 3D tomographic velocity analysis of residual moveout in prestack depth-migrated common image point gathers: 68th Annual International Meeting, SEG, Expanded Abstracts, 1218–1221.